This is the Pre-Published Version.

1

A NOVEL NONCONTACT ULTRASOUND INDENTATION SYSTEM

FOR MEASUREMENT OF TISSUE MATERIAL PROPERTIES

USING WATER JET COMPRESSION

5

M.H. Lu, Y.P. Zheng and Q.H. Huang

Jockey Club Rehabilitation Engineering Center, the Hong Kong Polytechnic University,

Kowloon, Hong Kong SAR, China.

9

10

Running Title: **Ultrasound Water Jet Indentation System**

12

13

Corresponding author:

Yongping Zheng

Jockey Club Rehabilitation Engineering Center,

The Hong Kong Polytechnic University,

Hung Hom, Kowloon, Hong Kong SAR, P. R. China.

Tel: 852-27667664

Fax: 852-23624365

Email: ypzheng@ieee.org

22

23

0

1 **A NOVEL NONCONTACT ULTRASOUND INDENTATION SYSTEM**

2 **FOR MEASUREMENT OF TISSUE MATERIAL PROPERTIES**

3 **USING WATER JET COMPRESSION**

4 M.H. Lu, Y.P. Zheng and Q.H. Huang

5 Jockey Club Rehabilitation Engineering Center, The Hong Kong Polytechnic University,

6 Kowloon, Hong Kong SAR, China.

7 **Abstract**

8   This study is aimed to develop a novel noncontact ultrasonic indentation system

9 for measuring quantitative mechanical properties of soft tissues, which are increasingly

10 important for tissue assessment and characterization. The key idea of this method is to

11 use a water jet as an indenter to compress the soft tissue while at the same time as a

12 medium for an ultrasound beam to propagate through. The use of water jet indentation

13 does not require a rigid compressor in front of the focused high frequency ultrasound

14 transducer to compress the tissue, so that the additional attenuation caused by the rigid

15 compressor and the strong echoes reflected from its surfaces can be avoided. The

16 indentation deformation was estimated from the ultrasound echoes using a cross-

17 correlation algorithm and the indentation force was calculated from the water pressure

18 measured inside the water pipe. Experiments were performed on uniform tissue-

19 mimicking phantoms with different stiffness. The Young's moduli and Poisson's ratios of

20 these phantoms were measured using a uniaxial ultrasound compression system. The ratio

21 of the indentation pressure to the tissue relative deformation was obtained from the water

22 indentation. This ratio was well correlated with the Young's modulus ($r=0.87$). The

23 results also demonstrated that the water indentation approach could differentiate materials

24 with different stiffness in a combined phantom (288 kPa and 433 kPa). This novel

25 noncontact water indentation approach could be potentially used for the measurement of

1 the elasticity of small samples and with a fast scanning speed. (E-mail:

2 ypzheng@ieee.org)

3 **Keywords:** ultrasound, high-frequency ultrasound, indentation, ultrasound indentation,

4 nanoindentation, noncontact, tissue, water jet.

5

6   **INTRODUCTION**

7   To measure or image the mechanical properties of tissues has been attracting

8 increasing research efforts during the recent decades. The stiffness of soft tissues may

9 change under different pathological situations, such as sclerous cancer, edema,

10 degeneration, fibrosis and pressure sore (Mridha and Odman 1986, Garra et al. 1997).

11 Normal tissues may also have different stiffness, which is important information for

12 tissue characterization. The mechanical properties of tissues can have different values

13 depending on whether they are measured *in vivo* or *in-vitro* and *in situ* or as an excised

14 specimen (Fung 1981, Mow and Hayes 1997). For the lack of quantitative tools for *in*

15 *vivo* assessment of living tissue, manual palpation has been the primary technique for

16 tissue stiffness assessment for many years in clinic. However, it strongly relies on

17 personal experiences and cannot provide a quantitative measurement of changes in tissue

18 stiffness.

19   Many mechanical methods, such as indentation, compression, tension and torsion,

20 are available quantitatively to measure the mechanical properties of soft tissues. Among

21 them, indentation is one of the most frequently used approaches. It does not require

22 special preparation for the specimens. Moreover, indentation can determine the material

23 properties of soft tissues *in situ* or *in vivo*. Theoretical analysis of general indentation

24 problems with various idealizations of the physical model has been conducted for about a

25 century. Some mathematical solutions have also been reported for thin-layer soft tissues

1   and materials using different mechanical model (Waters 1965; Hayes et al. 1972; Mak et

2   al. 1987; Mow et al. 1989; Chicot et al. 1996; Yu and Blanchard 1996; Sakamoto et al.

3   1996; Haider and Holmes 1997). The indentation depth, the shape and size of the indenter,

4   tissue thickness and the boundary conditions are critical factors in the calculation of

5   tissue mechanical properties (Jurvelin et al. 1990; Suh and Spilker 1994; Zhang et al.

6   1997; Yang 2003).

7   Several generations of indentation instruments have been developed for the

8   assessment of tissue mechanical properties, especially for articular cartilage (Kempson et

9   al. 1971; Hori and Mockros 1976; Mow et al. 1989; Newton et al. 1997; Arokoski et al.

10   1994, 1999; Athanasiou et al. 1995, 1999; Shepherd and Seedhom 1997). These

11   mechanical indentation apparatuses employ a load cell to measure the loading force and a

12   displacement transducer (LVDT) to record the tissue deformation according to the

13   displacement of the indenter. Cylindrical flat-ended and spherical indenters have been

14   used to perform contact loading on soft tissues. The structures of these mechanical

15   indentation instruments are complicated and not convenient for *in vivo* measurement. In

16   addition, these instruments employ a needle probe to penetrate into the cartilage to

17   measure the tissue thickness, which is important information for the estimation of

18   stiffness. Destruction of the tissue structure at the site of measurement restricts the further

19   use of the specimen. For clinical application, similar but portable indentation instruments

20   have been developed for the quantification of cartilage stiffness under arthroscopic

21   control (Lyyra et al. 1995), *in vivo* analysis of residual limb tissues (Pathak et al. 1998),

22   plantar tissue stiffness measurement in patients with diabetes mellitus and peripheral

23   neuropathy (Klaesner et al. 2002), stiffness estimation of spinal tissues (Kawchuk and

24   Fauvel 2001) and heel pad stiffness assessment (Rome and Webb 2000). These

25   indentation apparatuses use the obtained force/deformation (F/D) curves to indicate the

3

1   tissue stiffness. However, the obtained stiffness may depend on the tissue thickness,

2   which cannot be measured using these instruments.

3   During recent decades, ultrasound techniques together with compression or

4   indentation have been successfully used for the measurement or imaging of the

5   mechanical properties of soft tissues (Wilson and Robinson 1982; Ophir et al. 1991,

6   Zheng and Mak 1996, Hsu et al. 1998, Adam et al. 1998, Suh et al. 2001, Kawchuk et al.

7   2000, Laasanen et al. 2002, Han et al. 2003). The ultrasound indentation apparatuses can

8   simultaneously measure the tissue thickness and the tissue deformation *in vivo*

9   noninvasively. A load cell or a strain gauge integrated with a flat-ended ultrasound

10   transducer is used to collect the load applied on the tissue. In ultrasound indentation, the

11   ultrasound transducer also serves as the indenter. The accuracy of ultrasonically-

12   measured displacement during indentation has been earlier investigated (Zheng and Mak

13   1996, Kawchuk and Elliott 1998, Kawchuk et al. 2000). Compared with other methods,

14   such as those using optical (Jurvelin et al. 1997) and needle probe (Mow et al. 1989)

15   based methods, ultrasound-based techniques have proven to be most suitable for *in vivo*

16   tissue thickness measurement, because of their noninvasiveness. Ultrasound indentation

17   is easy to use for *in vivo* stiffness measurement and it has been widely used for

18   assessment of normal limb tissues (Zheng and Mak 1999a, 1999b), residual limb tissues

19   (Zheng et al. 1999), diabetic foot tissue (Zheng et al. 2000a, Hsu et al. 2000), fibrotic

20   neck tissue induced by radiotherapy (Zheng et al. 2000b; Leung et al. 2002), spinal

21   tissues (Kawchuk et al. 2001) and articular cartilage (Suh et al. 2001; Laasanen et al.

22   2002).

23   Present ultrasound indentation techniques utilize an unfocused transducer as the

24   indenter to compress the soft tissue. Direct contact between the transducer and the

25   specimen makes it difficult for them properly to compress small tissue specimens, due to

4

1 the relatively large size of the transducer. Moreover, the reported ultrasound indentation

2 device typically operated in the ultrasound frequency range of 2 MHz to 10 MHz. The

3 resolution is not sufficient for the measurement and imaging of the mechanical properties

4 of tissues with fine structures, such as articular cartilage (Zheng et al. 2002), corneal

5 tissues (Hollman et al. 2002) or skin (Zheng et al. 2004). To achieve ultrasound

6 indentation measurement at a microscopic level, ultrasound transducers with high

7 frequency have to be used. An additional rigid compressor or indenter between the

8 concave-faced focused transducer and the specimen is necessary for present techniques.

9 The rigid indenter will attenuate the ultrasound signal significantly and generate multiple

10 reflection signals which could overlap with signals from the specimen (Zheng et al. 2002,

11 2004). In addition, a contact compression or indentation could not allow for a fast

12 scanning for a region of tissues. Accordingly, it is very necessary to develop a new

13 method to achieve noncontact ultrasound indentation so that we can 1) perform proper

14 loading on small specimen, 2) use high frequency ultrasound without the problem of high

15 attenuation and 3) conduct a fast scanning to map tissue properties. Water jet acoustic

16 coupling is well known in the nondestructive evaluation field for quality control (Birks

17 and Green 1991; Zhao et al. 2003). Our approach is based on this technique. The key idea

18 is to use a water jet simultaneously as the indenter and the medium for ultrasound to

19 propagate through, so as to measure or map the mechanical properties of tissues. The

20 potential of this noncontact ultrasound indentation system quantitatively to measure the

21 phantoms with different stiffness is demonstrated in the following sections.

22
23
24 **MATERIALS AND METHODS**

25 **Water indentation system**

26   A noncontact ultrasound indentation system was constructed (Fig. 1), using a

1   water jet as an indenter. As shown in Fig. 1, a bubbler (B120, GE Panametrics, Inc., West

2   Chester, OH, USA) was used to eject a water jet by controlling the water flow. The

3   diameter of the water-ejecting nozzle was 1.94 mm. A 20 MHz focused ultrasound

4   transducer (model V316B, GE Panametrics, Inc., West Chester, OH, USA) was fixed

5   with the bubbler, i.e., the water ejector and the focused ultrasound beam could propagate

6   through the bubbler when it was full of water as coupling medium. The transducer and

7   the bubbler were installed to a three-dimensional translating device (Parker Hannifin

8   Corporation, Irvine, CA, USA) which was used to adjust the distance from the nozzle to

9   the specimen surface and later was used to perform one-dimensional or two-dimensional

10   scanning over the tissue. Specimens were placed on a rigid platform within a water

11   container. An outlet on the side of the container was used to control the water level. A

12   pressure sensor (EPB-C12, Entran Devices, Inc., Fairfield, NJ, USA) was used to

13   measure the water pressure within the water pipe. A load cell (ELFS-T3M, Entran

14   Devices, Inc., Fairfield, NJ, USA) located under the platform could sense the overall

15   force applied on the specimen.

16   An ultrasound pulser/receiver (model 5052 UA, GE Panametrics, Inc. West

17   Chester, OH, USA) was utilized to drive the ultrasound transducer and to amplify the

18   received signal. The ultrasound echoes reflected from the specimen were digitized by a

19   high speed A/D converter with a sampling rate of 2 GHz (Gage CS82G, Gage Applied

20   Technologies, Inc., QC, Canada). The pressure and the force were collected by a data

21   acquisition card (DAQ 6024E, National Instruments Corp. Austin, TX, USA). Figure 2

22   shows the system diagram. A program has been developed in Microsoft VC++ to control

23   the 3D translating device and collect, process and display the ultrasound signal, together

24   with the force and the pressure, in real time during the indentation process. The user

25   interface of the software is shown in Fig. 3. The acquisition of the A-mode ultrasound,

6

1 force and pressure data was synchronized by the program. All the data could be recorded

2 in a file for further off-line analysis. The deformation of the specimen under water jet

3 indentation was estimated from the ultrasound echoes using a cross-correlation algorithm

4 (Zheng et al. 2002). With the high-speed A/D converter, when the sampling frequency of

5 500 MHz was selected, the sensitivity of the time measurement was 2 ns. The theoretical

6 sensitivity of the deformation determined by the water indentation system was better than

7 4 μm (Zheng et al. 2004). By using the 24-bit A/D converter to digitize the force and

8 pressure signals, the accuracy of force was better than 1 μN within the 10 N range and the

9 accuracy of pressure was better than 0.05 Pa within the 350 kPa range.

10   The pressure sensor was used to measure and monitor the water pressure within the

11 water pipe. It was calibrated using a blood pressure meter with a range of 45 kPa and at a

12 sensitivity of 0.13 kPa. The load cell could sense the overall force applied on the platform

13 that was directly related to the force applied on the specimen by the water jet. It was

14 calibrated by using an electronic balance with a range of 1 N and at a sensitivity of 0.1

15 mN. Both the pressure and the force were used to derive the pressure applied on the

16 specimen by the water jet. The relationship between the overall force applied on the

17 platform and the pressure within the water pipe was studied when the distance from the

18 nozzle to the surface of the platform was fixed at approximately 5 mm, according to the

19 focal length of the focused ultrasound transducer. A linear regression was used to study

20 their relationship.

21

22 **Phantom preparation**

23   It has been reported that tissue-mimicking phantoms made from silicones or gels

24 have similar mechanical properties with soft tissues and their shapes, sizes and

25 compositions are easier to control (Hall et al. 1997). In our experiments, Rhodia RTV

7

1 573 (Rhodia Inc. CN7500, Cranbury, NJ, USA) and Wacker M4648 and M4640 silicones

2 (Wacker Chemicals Hong Kong Ltd., HK, China) were used to make phantoms with

3 different stiffness (Fig. 4). The uniform phantom was made from one kind of silicone and

4 was supposed to be homogeneous. The combined phantom was made from two kinds of

5 silicones, which had different stiffness at different areas. The sizes of the uniform

6 phantoms were $1\times1\times0.5$ cm^3 (width$\times$length$\times$height), $1\times1\times1$ cm^3, $1\times1\times1.5$ cm^3. The

7 combined phantoms had a height of 0.5 cm and a diameter of 2.2 cm.

8

9 **Experiment design for the uniform phantom**

10 To demonstrate the feasibility and the function of the noncontact ultrasound

11 indentation system, experiments were performed on phantoms and the

12 pressure/deformation curves were obtained. Galbraith and Bryant (1989) reported that the

13 results of the indentation analysis were unaffected if the lateral dimension of the tissue

14 was three or more times larger than the radius of the indenter. In this study, the lateral

15 dimension of the phantom (1×1 cm^2) was more than five times the radius of the water

16 indenter and the indentation was usually performed at the center of the phantom. During

17 the test, the phantom was placed at the center of the platform and was gently fixed at

18 edges by four screws. The position of the ultrasound transducer to the phantom surface

19 was adjusted according to the height of the phantom, so as to keep a constant initial

20 distance between the transducer and the phantom surface. The focal point of the

21 transducer was placed approximately at the surface level of the phantom. The distance

22 between the nozzle and the surface of the specimen was 5 mm. The container was full of

23 water before loading and a constant water level was kept during the test. In each loading

24 and unloading cycle, the water pressure within the water pipe was changed at a rate of

1   approximately 45 kPa/s and from 0 to 180 kPa, which corresponds to the local

2   deformation from 0 to approximately 0.4 mm for the softest phantom that we used. This

3   process was repeated for three cycles in each test. Each phantom was indented three

4   times. A total of 27 pieces of uniform phantoms were tested.

5

6   **1-D scanning on the combined phantom**

7   One-dimensional scanning experiment was conducted on the combined phantom,

8   using the three-dimensional translating device. The phantom was first scanned by the

9   ultrasound transducer at a moving rate of 1 mm/s when the pressure was kept as 0 kPa.

10   Then it was scanned again along the same line after the pressure changed to 58 kPa. The

11   deformation of the phantom at each site along the scanned line was obtained.

12

13   **Measurement of mechanical properties of phantoms**

14   As a reference of the experimental results of the water indentation, the

15   compressive properties of the phantoms were measured using a mechanical testing device

16   as shown in Fig. 5 (Zheng et al. 2002). The axial displacement was monitored by a

17   displacement transducer-linearly variable differential transformer (LVDT) and the lateral

18   deformation of the phantom was measured by an unfocused ultrasound transducer (5

19   MHz, model V316B, GE Panametrics, Inc. West Chester, OH, USA) during the axial

20   compression. Similar technique for measuring the lateral displacement of articular

21   cartilage has been reported by Fortin et al. (2003). Ultrasound coupling gel was used

22   between the ultrasound transducer and the phantom for ultrasound beam propagation. It

23   was also used in the interface between the phantom and the compressor and that between

24   the phantom and the platform, serving as lubrication. The phantom was placed at the

25   center of the platform and kept perpendicular to the ultrasound transducer by moving the

1   phantom to obtain a maximal ultrasound echo reflected from the two opposite surfaces of

2   the phantom. The ultrasound echoes were tracked using the cross-correlation algorithm to

3   estimate the lateral deformation of the phantom during compression. The uniaxial force

4   applied on the phantom was measured by a load cell (ELFS-T3M, Entran Devices, Inc.,

5   Fairfield, NJ, USA, calibrated for a range of 10 N). The axial displacement, force and

6   ultrasound echoes were recorded synchronously by the program. The compressive

7   Young's modulus and Poisson's ratio of the phantoms could be thus obtained.

8   The compressive Young's modulus of the phantom was calculated using eqn (1):

9    $$E = \frac{F/A}{\Delta L/L_0} \tag{1}$$

10   where E is the compressive Young's modulus of the phantom, F is the axial force applied

11   on the phantom, A is the surface area of the phantom, ΔL is the axial deformation and L_0

12   is the initial height of the phantom.

13   The Poisson's ratio calculation was based on the lateral deformation estimated

14   from the ultrasound echoes and the axial deformation measured by LVDT (eqn (2)). A

15   similar approach for the measurement of Poisson's ratio of articular cartilage using

16   optical detection has been reported earlier (Jurvelin et al. 1997).

17   $$\upsilon = \frac{\Delta W/W_0}{\Delta L/L_0} = \frac{|W_1 - W_0|/W_0}{|L_1 - L_0|/L_0} \tag{2}$$

18   where $W_0 = \frac{1}{2}t_1 \cdot c_{phantom}$, $W_1 = \frac{1}{2}t_2 \cdot c_{phantom}$, $\Delta W = W_1 - W_0 = \frac{1}{2}(t_2 - t_1) \cdot c_{phantom}$, where υ

19   is the Poisson's ratio of the phantom, ΔW is the lateral deformation, ΔL is the axial

20   deformation, W_0 and L_0 are the initial width and height of the phantom, t_1 and t_2 are the

21   time of flight of ultrasound between the two lateral faces of the phantom before and after

1   compression, respectively, and $c_{phantom}$ is the speed of sound in phantom. The meanings

2   of these variables are shown in Fig. 6.

3   The test for each phantom included loading and unloading phases. The test was

4   repeated three times on each phantom. The compression rate was kept at approximately

5   45 μm/s and the total deformation was up to 10%. Only the data with deformation less

6   than 3% were used to calculate the Poisson's ratio and Young's modulus, corresponding

7   to the 3% local strain of the phantoms under water indentation. According to the

8   stress/strain curves of the phantoms obtained from compression, they were in the linear

9   elastic region for the 3% deformation.

10

11   **RESULTS**

12   The mechanical properties of the phantoms were found to be dependent on the

13   applied strain. Therefore, the Young's moduli and Poisson's ratios were measured at the

14   strain according to the indentation depth on each phantom by using the noncontact water

15   indentation system. The results showed a good repeatability with ICC=0.99 (intraclass

16   correlation coefficient, SPSS Inc. Chicago, IL, USA) for the measurement of Young's

17   moduli and ICC=0.98 for the measurement of Poisson's ratio, respectively. The Young's

18   modulus of the phantoms ranged from 273 to 522 kPa and their Poisson's ratio ranged

19   from 0.26 to 0.44. It was noted that the phantoms could have different moduli, even when

20   they were made from the same silicone materials.

21   The calibration measurements indicated highly linear responses for both pressure

22   and force transducers ($R^2 = 0.999$ for the pressure sensor; $R^2 = 0.998$ for the load cell).

23   Moreover, it was found that there was a linear relationship ($R^2 = 0.99$) between the force

24   applied on the platform collected by the load cell and the water pressure within water

1   pipe measured by the pressure sensor (Fig. 7). Such a relationship will help us to

2   investigate the pressure applied on the phantom surface. At present, the average pressure

3   at the interface was calculated by the overall force divided by the initial contact area at

4   the interface.

5   Figure 8a shows the pressure/deformation curves during the loading and

6   unloading cycles applied on the phantom A and Fig. 8b shows the relationship between

7   the pressure and the surface deformation of the phantom. The relationship between the

8   deformation of the phantom and the applied water pressure loading was linear and the

9   data were fitted using linear regression (average $R^2 = 0.99$). The obtained slope, i.e., the

10 ratio of the applied pressure to the relative deformation, was defined as the stiffness ratio

11 of the phantoms, with a unit of kPa. The measurements of the stiffness ratio of the

12 phantoms showed a good repeatability (*ICC*>0.99) for the three tests. The stiffness ratio

13 of the phantoms ranged from 1582 to 4269 kPa.

14   A good linear relationship between the compressive Young's moduli and the

15 stiffness ratios was found with the correlation coefficient $r = 0.87$ ($n = 27$) (Fig. 9). This

16 result demonstrated that the ultrasound water indentation system had the ability

17 quantitatively to measure the phantoms with different stiffness. We estimated the

18 Young's modulus, E_w, from the obtained relationship between the stiffness ratio and the

19 compressive Young's modulus, *E,* of the phantoms. A Bland-Altman plot (Fig. 10) was

20 added to give indication of the size of errors between E_w and *E*. The mean difference

21 $\bar{d}$ was 0.02 kPa and the standard deviation *s* was 35.43 kPa. From the Bland-Altman plot,

22 most of the differences lay between $\bar{d}$ - *2s* and $\bar{d}$ + *2s*. The result was acceptable for

23 clinical applications (Bland and Altman, 1986). The thickness of the phantom was also

24 significantly ($P < 0.001$, linear regression by SPSS) correlated with the Young's modulus.

1 Moreover, significant correlation between the stiffness ratios and the square of Poisson's

2 ratios was found ($P = 0.04$). However, the extraction of the intrinsic mechanical

3 properties of the test materials from the water indentation needs further investigations.

4   Figure 11a shows the comparison of the M-mode ultrasound images obtained

5 under two different pressures (0 and 58 kPa). It could be observed that the surface of the

6 combined phantom was not flat. Figure 11b is the deformation distribution along the

7 scanned line derived from Fig. 11a. The result showed that, under a certain pressure, the

8 deformation of the region made from material A was larger than that made from material

9 B, i.e., the region made from material A was softer than that made from material B. The

10 Young's modului of these two regions were 288±2 and 433±5 kPa, respectively. The

11 measured deformation distribution under a certain pressure well demonstrated the

12 stiffness distribution of the combined phantom. We used this preliminary result to

13 demonstrate the feasibility of using the water indentation to map the distribution of the

14 stiffness ratio of soft tissues.

15

16   **DISCUSSION AND CONCLUSION**

17   A noncontact ultrasound indentation system using water jet has been developed

18 for the assessment of tissue mechanical properties. Preliminary results have demonstrated

19 that this novel system was feasible quantitatively to measure silicone phantoms with

20 different stiffness. As a water jet was used simultaneously as the indenter and the

21 medium for coupling the ultrasound beam, the system could obtain better ultrasound

22 echoes using focused high frequency ultrasound in comparison with the contact methods,

23 where rigid indenters or compressors were used to compress the tissue. It could also

24 conduct proper loading on small specimen, because of the small dimension of the water

25 indenter. Moreover, this water jet indentation system demonstrated its potential to

1   conduct fast scanning on specimens to map the deformation distribution.

2   In our experiments, a 20 MHz focused ultrasound transducer was used and the

3   system could achieve high axial resolution of the measurement because the deformation

4   of phantom under water indentation was determined from ultrasound echoes. For 20 MHz

5   ultrasound using in this study, two cycles of damping period and an ultrasound speed of

6   1480 m/s (Krautkramer and Krautkramer 1969), the theoretical axial resolution was

7   approximately 58 μm (Bushong and Archer 1991, Foster et al. 2000). The focal length of

8   the transducer was 19.05 mm, and the diameter of the active element of this transducer

9   was 3.175 mm. Therefore, the f-number (focal length/crystal diameter) was 6. The

10   theoretical lateral resolution was 0.44 mm (Foster et al. 2000). The resolutions could be

11   further improved by using higher frequency ultrasound. According to the numerical

12   simulation results, Righetti et al. (2002, 2003) and Srinivasan et al. (2003) reported that

13   the lateral and axial resolution limits of the strain images obtained using ultrasound were

14   on the order of the sonographic lateral resolution and the ultrasonic wavelength,

15   respectively. In the future study on the small specimen of soft tissues, a focused 50 MHz

16   ultrasound transducer will be used and it can achieve a theoretical axial resolution of 35

17   μm, and lateral resolution of 90 μm (Zheng et al. 2004). With further improvement of the

18   system, it is feasible to perform nanoindentation (Pethica et al. 1983) using the water

19   indentation. In the present study, we have only focused on the ultrasound echoes reflected

20   from the phantom surface, from which the overall deformation was derived. For the

21   tissues with multilayer or inhomogeneous structures, echoes from different depths can be

22   tracked during water indentation so as potentially to map the tissue stiffness in the depth

23   direction. Further experiments are required to validate the stiffness distribution using

24   proper techniques such as the optical elastomicroscopy system (Huang et al. 2004).

25   In our experimental set-up, daily tap water (24.2±0.2ºC) was used for the water

14

1   indentation system. We are planning to use a water pump, so that the water flow can be

2   better controlled. As the medium for ultrasound propagation was flowing during the

3   water indentation, the effect of the flow rate on the ultrasound speed had to be

4   investigated. Our result showed that the maximal change of the speed of sound through

5   water jet was less than 0.04% (0.6 m/s change for a speed of 1480 m/s) when the pressure

6   was changed from 0 to 180 kPa. The result suggested that the effect of water flow for

7   ultrasound speed could be neglected during the water indentation with the pressure up to

8   180 kPa. The water jet formed from the tap water might contain some amount of air

9   bubbles. The backscatter induced by these bubbles may attenuate the ultrasonic beam that

10 propagates through the water jet. It has been reported that the attenuation caused by the

11 air bubbles increases rapidly as the frequency is increased (Ophir and Parker 1989, Naito

12 et al. 1998, Phillips et al. 1998). However, the effects of the bubbles to the test proposed

13 in this study could be negligible according to our measurement. No dramatic attenuation

14 and scattering was caused by the air bubbles in the set-up used in this study. For the 20

15 MHz ultrasonic beam, we noted that the ultrasound echo from a steel plate located at the

16 focal zone was attenuated by less than -0.6 dB when the water flow was adjusted from 0

17 to the maximum value that used in this study. Such a small attenuation to the echo was

18 negligible in this study, as the main information involved in the calculation of the

19 deformation was the flight-time of the echo reflected from the surfaces of the phantom.

20   During our experiments, the ratio between the pressure and the relative

21 deformation curves was used as the index of the material stiffness. The stiffness ratio had

22 a good linear relationship (with correlation coefficients larger than 0.8) with the

23 measured compressive Young's modulus. This correlation may not be good enough for a

24 very precise measurement. However, the result demonstrated the feasibility of the new

25 ultrasound water jet system to measure the stiffness of the phantoms quantitatively. The

1   result of Bland-Altman plot (Fig. 10) demonstrated that the results were acceptable for

2   clinical applications (Bland and Altman, 1986).

3   However, the extraction of the intrinsic mechanical properties from the

4   noncontact water indentation needs further investigation. As previous investigations have

5   suggested (Waters, 1965; Hayes et al. 1972; Mak et al. 1987; Mow et al. 1989; Chicot et

6   al. 1996; Yu and Blanchard, 1996; Sakamoto et al. 1996; Haider and Holmes, 1997), the

7   Young's modulus derived from indentation test using a cylindrical indenter is related to

8   the Poisson's ratio of the material, stress distribution, indentation depth and tissue

9   thickness. Moreover, when soft tissues are tested for the measurements of mechanical

10   properties, the nonlinearity, viscoelasticity, nonhomogenuity and anisotropy should be

11   carefully considered for the mechanical properties' extraction. In this study, as the first

12   step, we tested silicone phantoms with uniform structures. The applied deformation was

13   within 3% and the loading cycle was completed within 4 s, so as to reduce the effects of

14   nonlinearity and viscoelasticity. We used the slope of the pressure/ relative deformation

15   curve instead of the pressure/ deformation curve to correlate with the Young's modulus,

16   since we found that the thickness of the phantoms was also well correlated with their

17   stiffness. Moreover, significant correlation between the stiffness ratio and square of

18   Poisson's ratio was also found. These observations will benefit us further to investigate

19   the extraction of intrinsic material parameters from the water indentation results.

20   However, we were not able yet to obtain a suitable equation precisely to describe the

21   relationship between the Young's modulus and the Poisson's ratio, tissue thickness, as

22   well as the applied pressure and the indentation depth using our experimental data.

23   The major cause of the discrepancy between the stiffness ratios measured using the

24   water jet indentation method and the Young's moduli measured using the compression

25   method may be the simplification in modeling the interaction between the water jet and

16

the phantom surface. It is expected that the deformation profile as well as the pressure distribution along the interacting interface keeps changing as the increase of the water jet pressure. We have tried different methods to measure the deformation profile and the pressure distribution. However, no satisfactory results have been obtained yet. In addition to improving our experimental approaches, we are also planning for the numerical analysis of the interaction between the water jet and the tissue. Finite element analysis is an effective tool and it has been employed to study the indentation problem (Galbraith and Bryant 1989; Jurvelin et al. 1990; Zhang et al. 1997; Lu and Zheng 2004). Using finite element analysis, we expect that the effects of the variations of the water jet radius, the distance from the nozzle to the phantom surface, the phantom thickness and the Poisson's ratio and the fluid-solid coupling motion can be studied. The interaction between the water jet and the tissue can be better investigated.

This noncontact ultrasound water indentation system has many potential applications. With further improvement of the system and better understanding about the water jet-tissue interaction, we expect that the water indentation approach could be potentially used quantitatively to assess the stiffness of body tissues for clinical diagnosis, such as skin cancer, burn status, cornea condition, blood vessel stiffening, articular cartilage degeneration etc. It could also be employed to perform indentation on small specimens in microscopic levels for tissue and material characterization for small animal tissues, bioengineered tissues, semiconductor materials, thin films and so on, where nanoindentation is widely used. Moreover, the potential fast scanning feature of the water indentation makes it easy to conduct scanning on tissues with large area.

Acknowledgements

3

4

5

6

7

8

9

10

11

12

13

14

15

16

17

18

19

20

21

22

23

24   **REFERENCES**

1   Adam C, Eckstein F, Milz S, Schulte E, Becker C and Putz R. The distribution of

2   cartilage thickness in the knee-joints of old-aged individuals - measurement by A-mode

3   ultrasound. Clin Biomech 1998; 13: 1-10.

4   Arokoski JPA, Hyttinen MM, Helminen HJ and Jurvelin JS. Biomechanical and

5   structural characteristics of canine femoral and tibial cartilage. J Biomed Mater Res

6   1999; 48: 99-107.

7   Arokoski J, Jurvelin J, Kiviranta I, Tammi M and Helminen HJ. Softening of the lateral

8   condyle aricular-cartilage in the canine knee-joint after long-distance (up to 40 km/day)

9   running training lasting one-year. Int J Sports Med 1994; 15: 254-260.

10 Athanasiou KA, Agarwal A, Muffoletto A, Dzida FJ, Constantinides G and Clem M.

11 Biomechanical properties of hip cartilage in experimental animal-models. Clin Orthop

12 Relat R 1995; 316: 254-266.

13 Athanasiou KA, Fleischli JG, Bosma J, et al. Effects of diabetes mellitus on the

14 biomechanical properties of human ankle cartilage. Clin Orthop Relat R 1999; 368:

15 182-189.

16 Birks AS and Green RE. Ultrasonic testing: nondestructive testing handbook. 1991;

17 Columbus, OH: American Society for Nondestructive Testing, Inc.

18 Bland JM and Altman DG. Statistical methods for assessing agreement between two

19 methods of clinical measurement. Lancet 1986; i: 307-310.

20 Bushong SC and Archer BR. Diagnostic ultrasound: physics, biology, and

21 instrumentation, 1991; New York: Mosby..

22 Chicot D, Hage I, Demarecaux P and Lesage J. Elastic properties determination from

23 indentation tests. Surf Coat Tech 1996; 81: 269-274.

24 Galbraith PC and Bryant JT. Effect of grid dimensions on finite element models of an

25 articular surface. J Biomech 1989; 22: 385-393.

1   Garra BS, Cespedea EI, Ophir J, Spratt RS, Zuurbier RA, Magnant CM, and Pennanen

2   MF. Elastography of breast lesions: initial clinic results. Radiology 1997; 202: 79-86.

3   Fung YC. Biomechanical properties of living tissues. 1981; Springer-Verlag, New York.

4   Foster FS, Pavlin CJ, Harasiewicz KA, Christopher DA, and Turnbull DH. Advances in

5   ultrasound biomicroscopy. Ultrasound Med Biol 2000; 26: 1-27.

6   Fortin M, Buschmann MD, Bertrand MJ, Foster FS, and Ophir J. Dynamic measurement

7   of internal solid displacement in articular cartilage using ultrasound backscatter. J

8   Biomech 2003; 36: 443-447.

9   Haider MA and Holmes MH. A mathematical approximation for the solution of a static

10   indentation test. J Biomech 1997; 30: 747-751.

11   Hall TJ, Bilgen M, Insana MF and Krouskop TA. Phantom materials for elastography.

12   IEEE T Ultrason Ferr 1997; 44: 1355-1365.

13   Han LH, Noble JA and Burcher M. A novel ultrasound indentation system for measuring

14   biomechanical properties of in vivo soft tissue. Ultrasound Med Biol 2003; 29: 813-823.

15   Hayes WC, Herrmann G, Mockros LF and Keer LM. A mathematical analysis for

16   indentation tests of articular cartilage, J Biomech 1972; 5: 541-551.

17   Hollman KW, Emelianov SY, Neiss JH, et al. Strain imaging of corneal tissue with an

18   ultrasound elasticity microscope. Cornea 2002; 21: 68-73.

19   Hori RY and Mockros LF. Indentation tests of human articular-cartilage. J Biomech 1976;

20   9: 259-268.

21   Huang QH, Lu MH and Zheng YP. Optical and ultrasound elastomicroscopy for imaging

22   tissue elasticity in high resolution. Conference on Biomedical Engineering, BME 2004,

23   23 -25 September 2004, Hong Kong: 130-134

24   Hsu TC, Wang CL, Shau YW, Tang FT, Li KL, Chen CY. Altered heel-pad mechanical

25   properties in patients with Type 2 diabetes mellitus. Diabet Med 2000; 17: 854-859.

1   Hsu TC, Wang CL, Tsai WC, Kuo JK, and Tang FT. Comparison of the mechanical

2   properties of the heel pad between young and elderly adults. Arch Phys Med Rehabil

3   1998; 79: 1101-1104.

4   Jurvelin J, Kiviranta I, Saamanen AM, Tammi M and Helminen HJ. Indentation stiffness

5   of young canine knee articular-cartilage – influence of strenuous joint loading. J

6   Biomech 1990; 23: 1239-1246.

7   Jurvelin JS, Buschmann MD and Hunziker EB. Optical and mechanical determination of

8   Poisson's ratio of adult bovine humeral articular cartilage. J Biomech 1997; 30: 235-

9   241.

10 Kawchuk GN and Elliott PD. Validation of displacement measurements obtained from

11   ultrasonic images during indentation testing. Ultrasound Med Biol 1998; 24: 105-111.

12 Kawchuk GN and Fauvel OR. Sources of variation in spinal indentation testing:

13   indentation site relocation, intraabdominal pressure, subject movement, muscular

14   response, and stiffness estimation. J Manip physiol ther 2001a; 24: 84-91.

15 Kawchuk GN, Fauvel OR and Dmowski J. Ultrasonic quantification of osseous

16   displacements resulting from skin surface indentation loading of bovine para-spinal

17   tissue. Clin Biomech 2000; 15: 228-233.

18 Kawchuk GN, Fauvel OR and Dmowski J. Ultrasound indentation: a procedure for the

19   noninvasive quantification of force-displacement properties of the lumber spine. J

20   Manip physiol ther 2001b; 24: 149-156.

21 Kempson GE, Freeman MAR and Swanson SAV. The determination of a creep modulus

22   for articular cartilage from indentation tests on human femoral head. J Biomech 1971; 4:

23   239-250.

1   Klaesner JW, Hastings MK, Zou DQ, Lewis C and Mueller MJ. Plantar tissue stiffness

2   in patients with diabetes mellitus and peripheral neuropathy. Arch Phys Med Rehabil

3   2002; 83: 1796-1801.

4   Krautkramer J and Krautkramer H. Ultrasonic testing of materials. 1969; New York:

5   Springer-Verlag.

6   Laasanen MS, Toyras J, Hirvonen J, et al. Novel mechano-acoustic technique and

7   instrument for diagnosis of cartilage degeneration. Physiol Meas 2002; 23: 491-503.

8   Leung SF, Zheng YP, Choi CYK, et al. Quantitative measurement of post-irradiation

9   neck fibrosis based on the Young modulus: description of a new method and clinical

10   results. Cancer 2002; 95: 656-662.

11   Lu MH and Zheng YP. Indentation test of soft tissues with curved cubstrates: a finite

12   element study. Med Biol Eng Comput 2004; 42: 535-540.

13   Lyyra T, Jurvelin J, Pitkanen P, Vaatainen U and Kiviranta I. Indentation instrument for

14   the measurement of cartilage stiffness under arthroscopic control. Med Eng Phys 1995;

15   17: 395-399.

16   Mak AF, Lai WM and Mow VC. Biphasic indentation of articular-cartilage .1. theoretical

17   -analysis. J Biomech 1987; 20: 703-714.

18   Mow VC, Gibbs MC, Lai WM, Zhu WB and Athanasiou KA. Biphasic indentation of

19   articular-cartilage .2. a numerical algorithm and an experimental-study. J Biomech

20   1989; 22: 853-861.

21   Mow VC and Hayes WC. Basic Orthopaedic Biomechanics. 2nd edition. 1997;

22   Lippincott-Raven.

23   Mridha M and Odman S. Noninvasive method for assessment of subcutaneous edema.

24   Med Biol Eng Comput 1986; 24: 393-398.

1   Newton PM, Mow VC, Gardner TR, Buckwalter JA and Albright JP. The effect of

2   lifelong exercise on canine articular cartilage. AM J Sport Med 1997; 25: 282-287.

3   Naito T, Ohdaira E, Masuzawa N, and Ide M. Relationship between cavitation threshold

4   and dissolved air in ultrasound in the MHz range. Jpn J Appl Phys 1998; 37: 2990-2991.

5   Ophir J, Ce´spedes I, Ponnekanti H, Yazdi Y and Li X. Elastography: a quantitative

6   method for imaging the elasticity of biological tissues. Ultrasonic Imaging 1991; 13:

7   111–134.

8   Ophir J and Parker KJ. Contrast agents in diagnostic ultrasound. Ultrasound Med Biol

9   1989; 15: 319-333.

10   Pathak AP, Silver-Thorn MB, Thierfelder CA and Prieto TE. A rate-controlled indentor

11   for in vivo analysis of residual limb tissues. IEEE T Rehabil Eng 1998; 6: 12-20.

12   Pethica JB, Hutchings R, and Oliver WC. Hardness measurement at penetration depths as

13   small as 20-nm. Philos Mag A 1983; 48: 593-606.

14   Phillips D, Chen XC, Baggs R, Rubens D, Violante M, and Parker KJ. Acoustic

15   backscatter properties of the particle/bubble ultrasound contrast agent. Ultrasonics 1998;

16   36: 883-892.

17   Righetti R, Ophir J, and Ktonas P. Axial resolution in elastography. Ultrasound Med Biol

18   2002; 28: 101-113.

19   Righetti R, Srinivasan S, and Ophir J. Lateral resolution in elastography. Ultrasound Med

20   Biol 2003; 29: 695-704.

21   Srinivasan S, Righetti R, and Ophir J. Trade-offs between the axial resolution and the

22   signal-to-noise ratio in elastography. Ultrasound Med Biol 2003; 29: 847-866.

23   Rome K and Webb P. Development of a clinical instrument to measure heel pad

24   indentation. Clin Biomech 2000; 15: 298-300.

1 Sakamoto M, Li GA, Hara T and Chao EYS. A new method for theoretical analysis of
2   static indentation test. J Biomech 1996; 29: 679-685.

3 Shepherd DET and Seedhom BB. Technique for measuring the compressive modulus of
4   articular cartilage under physiological loading rates with preliminary results. P I Mech
5   Eng H 1997; 211: 155-165.

6 Suh JK and Spilker RL. Indentation analysis of biphasic articular-cartilage – nonlinear
7   phenomena under finite deformation. J Biomech Eng- T ASME 1994; 116: 1-9.

8 Suh JKF, Youn I and Fu FH. An in situ calibration of an ultrasound transducer: a
9   potential application for an ultrasonic indentation test of articular cartilage. J Biomech
10   2001; 34: 1347-1353.

11 Waters NE. The indentation of thin rubber sheets by spherical indentors. Brit J Appl Phys
12   1965; 16: 557-563.

13 Wilson LS and Robinson DE. Ultrasonic measurement of small displacements and
14   deformations of tissue. Ultrasonic Imaging 1982; 4: 71–82.

15 Yang F. Thickness effect on the indentation of an elastic layer. Mat Sci Eng A 2003; 358:
16   226-232.

17 Yu WP and Blanchard JP. An elastic-plastic indentation model and its solutions. J Mater
18   Res 1996; 11: 2358-2367.

19 Zhang M, Zheng YP and Mak AFT. Estimating the effective Young's modulus of soft
20   tissues from indentation tests - nonlinear finite element analysis of effects of friction
21   and large deformation. Med Eng Phys 1997; 19: 512-517.

22 Zhao B, Basir OA, and Mittal GS. A self-aligning ultrasound sensor for detecting foreign
23   bodies in glass containers. Ultrasonics 2003; 41: 217-222.

1   Zheng YP, Bridal SL, Shi J, et al. High resolution ultrasound elastomicroscopy imaging

2   of soft tissues: system development and feasibility. Phys Med Biol 2004; 49: 3925-

3   3938.

4   Zheng YP, Choi YKC, Wong K, Chan S and Mak AFT. Biomechanical assessment of

5   plantar foot tissue in diabetic patients using an ultrasound indentation system.

6   Ultrasound Med Biol 2000a; 26: 451-456.

7   Zheng YP, Leung SF and Mak AFT. Assessment of neck tissue fibrosis using an

8   ultrasound palpation system: A feasibility study. Med Biol Eng Comput 2000b; 38:

9   497-502.

10   Zheng YP and Mak AFT. An ultrasound indentation system for biomechanical properties

11   assessment of soft tissues in-vivo. IEEE T Bio-Med Eng 1996; 43: 912-918.

12   Zheng YP and Mak AFT. Extraction of quasilinear viscoelastic parameters for lower limb

13   soft tissues from manual indentation experiment. J Biomech Eng- T ASME 1999a; 121:

14   330-339.

15   Zheng YP and Mak AFT. Effective elastic properties for lower limb soft tissues from

16   manual indentation experiment. IEEE T Rehabil Eng 1999b; 7: 257-267.

17   Zheng YP, Mak AFT, Lau KP and Qin L. An ultrasonic measurement for in vitro depth-

18   dependent equilibrium strains of articular cartilage in compression. Phys Med Biol

19   2002; 47: 3165-3180.

20   Zheng YP, Mak AFT and Lue B. Objective assessment of limb tissue elasticity:

21   development of a manual indentation procedure. J Rehabil Res Dev 1999; 36: 71-85.

22
23
24

25

26

1

2

3

4

5

6

7

8

9

10

11

12

13

14

15

16

17

18

19

20 **Figure Captions**

21 Fig. 1. Diagram of the noncontact ultrasound indentation system using water jet

22 compression. The water jet is used as an indenter and focused high-frequency ultrasound

23 is employed to monitor the deformation of the soft tissue. The dimensions of the

24 important components are: nozzle diameter 1.94 mm, water supply pipe diameter 3 mm,

25 platform diameter 24 mm, load cell diameter 12.7 mm, ultrasound transducer active

26

1 element diameter 3.175 mm and the distance from the nozzle to tissue approximately 5

2 mm.

3

4 Fig. 2. The water indentation and data collection diagram of the noncontact ultrasound

5 water indentation system.

6

7 Fig. 3. The user interface of the signal processing software. The left column is the control

8 panel, showing various parameters. In the main window, the lower right window displays

9 the real-time ultrasound signal reflected from the sample surface, the lower left windows

10 shows the force sensed by the load cell or pressure measured by the pressure sensor, the

11 upper left window shows the M-mode ultrasound signals and the upper right window is

12 the deformation extracted from the ultrasound signal using the cross-correlation tracking

13 algorithm.

14

15 Fig. 4. Phantoms made from three kinds of silicones were prepared for the experiments.

16 (a) The uniform phantoms with dimensions $1\times1\times0.5$ cm^3 (width×length×height), (b)

17 $1\times1\times1$ cm^3 and (c) $1\times1\times1.5$ cm^3. (d) The combined phantom with a height of 0.5 cm

18 and a diameter of 2.2 cm.

19 Fig. 5. Diagram of the system which was used to measure the compressive Young's

20 modulus and Poisson's ratio of the phantoms. A load cell was used to measure the

21 uniaxial force applied on the phantom. An ultrasound transducer was used to estimate the

22 lateral deformation of the phantom, while the LVDT was used to measure the axial

23 deformation.

24

1 Fig. 6. Schematic diagram for the estimation of the Poisson's ratio of the uniform

2 phantom. t_1 and t_2 are the times-of-flight of ultrasound from the two parallel surfaces of

3 the phantom before and after compression, respectively.

4

5 Fig. 7. The relationship between the force applied on the platform and the pressure

6 measured within the water pipe. The equation shows the result of a linear regression.

7

8 Fig. 8 (a). Pressure-deformation curves obtained during the loading and unloading cycles

9 applied on one uniform phantom. (b) The relationship between the pressure measured

10 within the water pipe and the relative deformation of the phantom.

11

12 Fig. 9. The correlation between the compressive Young's modulus and the stiffness ratio

13 obtained using the ultrasound water indentation (r=0.87, n=27).

14

15 Fig. 10. Bland-Altman plot to test the agreement between the estimated Young's modulus

16 by water indentation and the measured modulus by compression.

17

18 Fig. 11. A typical result of one-dimensional scanning on the combined phantom. (a)

19 Comparison of the M-mode ultrasound images obtained under two different pressures. (b)

20 The deformation distribution along the scanned line as derived from (a).

21

22

23

24

1

2

3

4

5

6

7

8

9

10

Figure 1.

11

12

13

14

15

1

2

3

4

Figure 2.

5

6

7

8

9

10
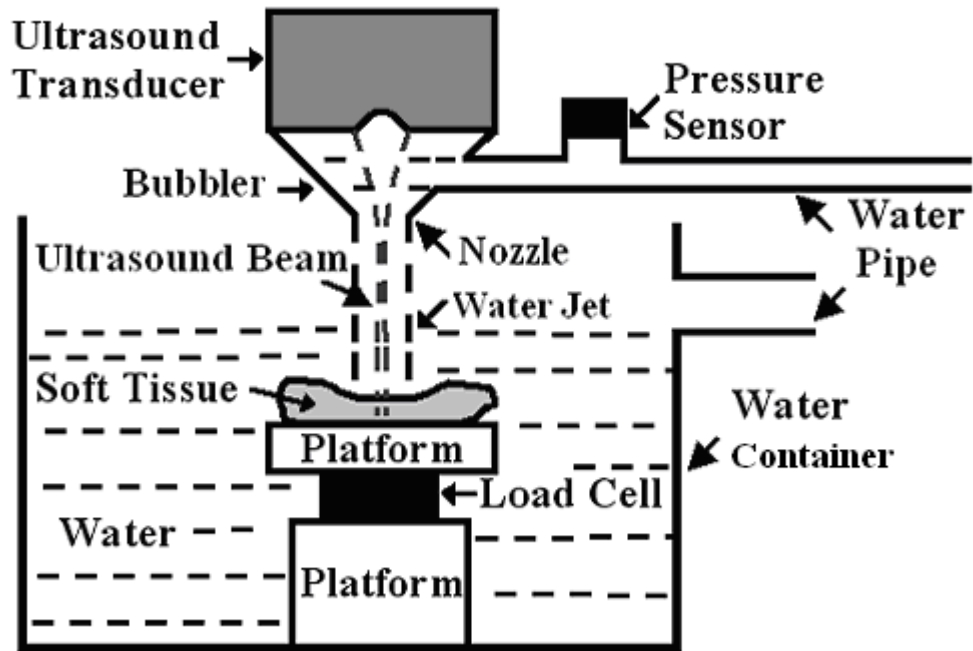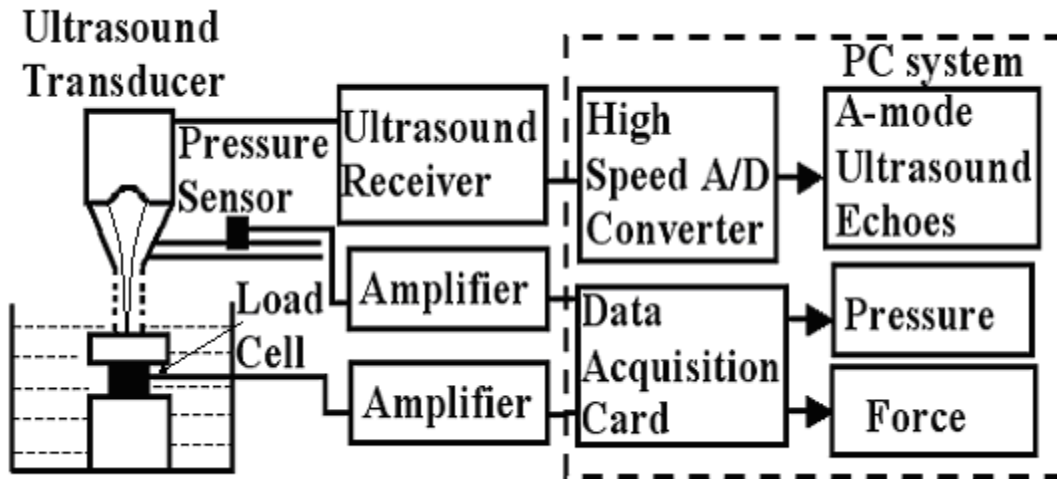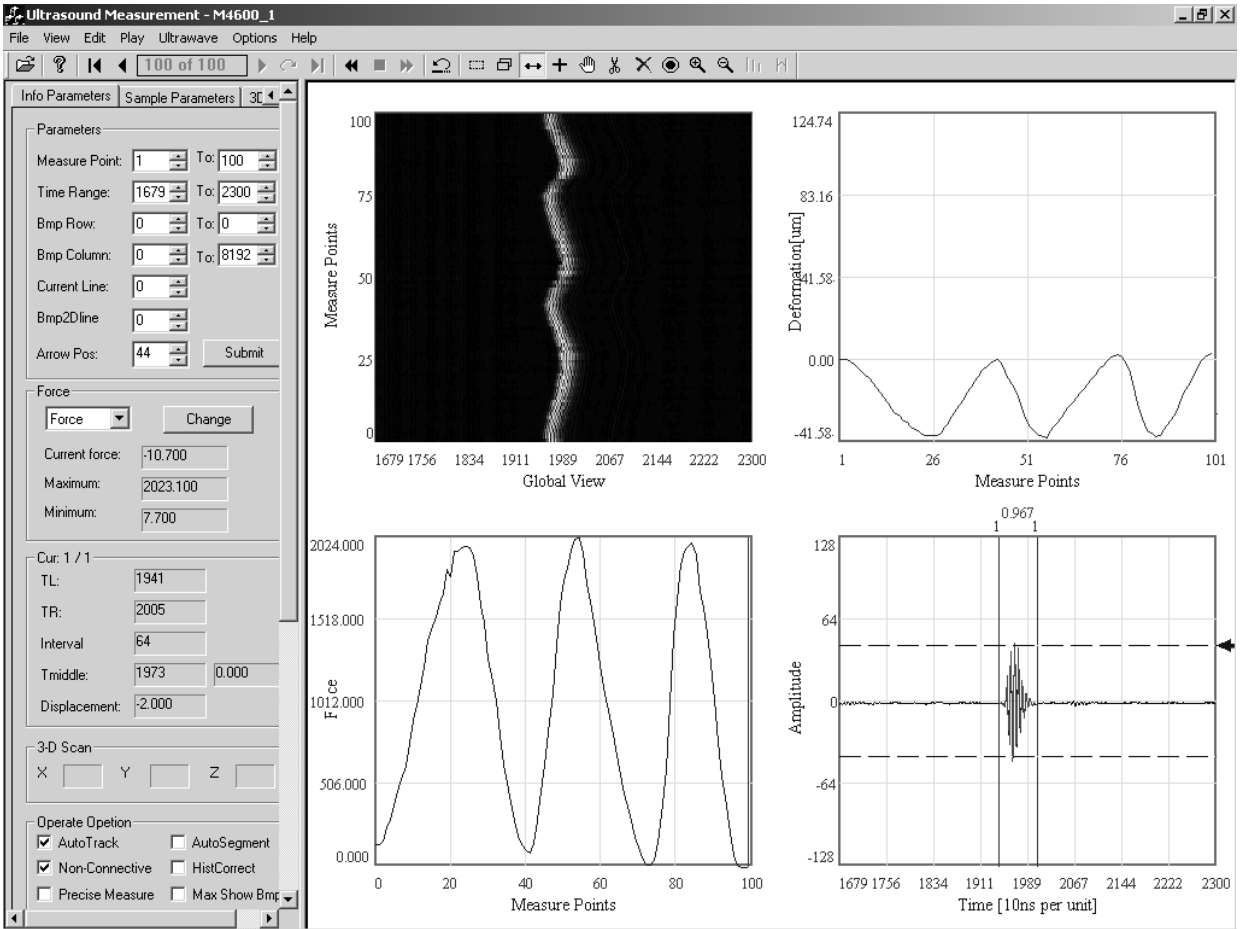
Figure 3.

Figure 4.

1
2
3
4
5
6
7
8
9
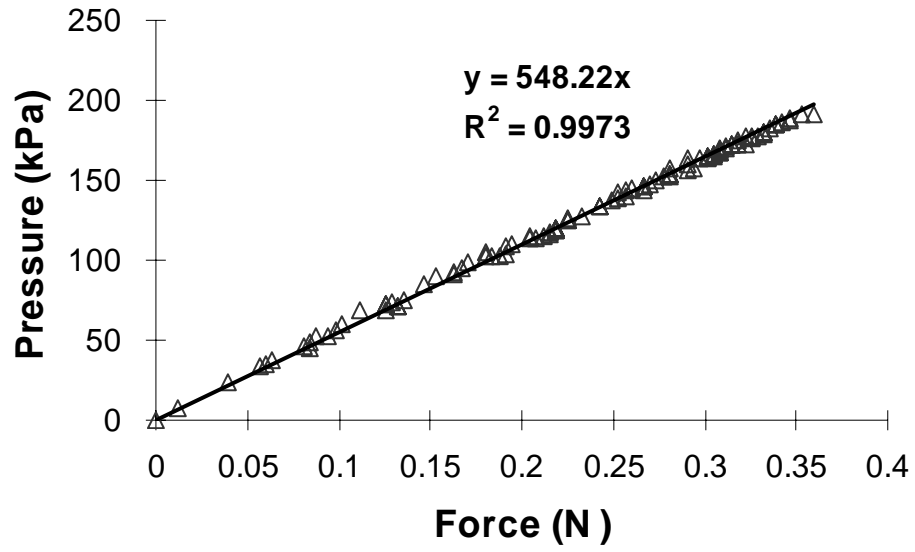10

Figure 5.

1

2

3

4

5

6

7

8

9

10

11

1

2   Figure 6.

3

y = 548.22x
R^2 = 0.9973

Pressure (kPa) vs Force (N)

1

2   Figure 7.

3

4

5

6

7

8

9

Figure 8 (a).

Figure 8 (b).

Figure 9.

1

2

3

4

5

6

7

8

9

Figure 10.

Echoes from the phantom surface

13 mm

4.5 mm

2.54 mm

0.55 mm

B　A　B

B　A　B

Pressure = 0

Pressure = 58 kPa

Figure 11 (a).

Figure 11 (b).